Simulation of an ac electro-osmotic pump with step microelectrodes

Byoung Jae Kim,[1,2] Seung-Hyun Lee,[3] Soghra Rezazadeh,[1] and Hyung Jin Sung[1,*]
[1]*Department of Mechanical Engineering, KAIST, Daejeon 305-701, Korea*
[2]*Thermal-Hydraulics Safety Research Division, KAERI, Daejeon 305-353, Korea*
[3]*Nano-Mechanical Systems Research Division, KIMM, Daejeon 305-343, Korea*
(Received 8 February 2011; revised manuscript received 28 March 2011; published 3 May 2011)

Pumps with step microelectrodes subjected to an ac voltage are known to have faster pumping rates than those with planar asymmetric microelectrodes. The driving force for pumping in these systems is ac electro-osmosis. This paper aims to understand the flow behaviors of pumps with step microelectrodes by using a realistic model applicable to high external voltages. This model takes the steric effect due to the finite sizes of ions into account and copes with the exponential sensitivity of the counterion concentration to voltage. The effects on the pumping flow rate of varying the pump parameters were investigated. The geometrical parameters were optimized, and the effects of varying the ac frequency and amplitude were examined. The electrical potential of the fluid and the electrical charge at the electrode surface were solved simultaneously, and the Stokes equation was used to describe the fluid flow.

DOI: 10.1103/PhysRevE.83.056302 PACS number(s): 47.57.jd, 47.65.−d, 47.61.Fg, 47.85.Np

I. INTRODUCTION

Over the last two decades, a variety of mechanical, chemical, or electrical methods for the transport of small amounts of liquid in microchannels has been proposed, with the aim of extending micropump applications to microfluidic devices [1]. The selection criteria for a micropump depend on the pumping mechanism that is suitable to the given application. Of these mechanisms, electrical approaches are attractive because of their easy realization, the absence of moving parts, and their compatibility with electrical devices. dc electro-osmosis is one such approach that is a well-known and simple phenomenon. In general, however, it requires high voltages (∼kV) to move fluids. At such high voltages, electrodes are subject to degradation, and boiling can occur. Instead of using dc voltages, electro-osmosis with ac voltages has recently received significant attention because of the remarkably low working voltages (∼V) required to move liquids in microchannels.

Early ac electro-osmotic pumps mostly adopted planar asymmetric microelectrode arrays. Ramos *et al*. [2] carried out a numerical study of electro-osmosis with planar asymmetric microelectrodes by using a linear capacitor model for the electrical double layer. Since that study, the linear model has been used as a standard tool for gaining qualitative insight into fluid flow [3]. The linear model is physically valid up to, at most, a few millivolts. However, ac electro-osmotic pumps practically require voltages of several volts. The linear model is not able to predict flow reversals that are experimentally observed at high frequencies and high voltages [4,5] and are not able to show the dependence of the electrical conductivity on the pumping flow rate. Moreover, the linear model is known to predict much higher fluid velocities than are found in experiments. Attempts have been made to develop models that overcome these limitations, in particular, that can describe the electrical double layers under high voltages [6–8]. One important consideration in these attempts is the effect of finite ion sizes, that is, the steric effect. Storey *et al*. [9] applied two steric effect models to pumps with planar asymmetric electrodes in which flow reversal was successfully predicted.

Meanwhile, an array with step microelectrodes was proposed that enhances the pumping flow rate [10]. The advantage of the step electrodes is that their flow is faster and more uniform. Urbanski *et al*. [11] performed a numerical study of these flow patterns using the linear model in which the effects of varying the step height were investigated. Recently, Huang *et al*. [12] experimentally demonstrated that the step electrodes could be an ultrafast and high-pressure pump, which is capable of transporting biological particles, such as DNA. Burch and Bazant [13] altered the boundary conditions of the step geometry; as a result, the pumping velocity was about twice as fast as the step electrode over the wide range of frequencies. The studies above relating to the step geometry utilized simulation results with the linear model for the double layer.

This paper aims for a more realistic simulation of pumps with step electrodes. In contrast to the previous studies, a nonlinear model was used that accounts for finite ion sizes; this modifies the classical Poisson-Nernst-Planck model. Simulations were performed with the aim of investigating the effects on the pumping flow rate of varying the geometrical parameters and the ac voltage. The electrical potential of the fluid and the electrical charge at the electrode surface were first solved simultaneously. The time-averaged slip velocity at the electrode surface was then calculated from the potential gradient and the charge. The fluid flow was then obtained by solving the Stokes equation with the time-averaged slip velocity.

II. SIMULATION METHODS

A. Simulation conditions

Figure 1 shows a schematic of the micro-electro-osmotic pump with step microelectrodes. A number of microelectrodes is placed periodically on the channel bottom, and two microelectrodes constitute one pair. When an ac voltage is

*hjsung@kaist.ac.kr

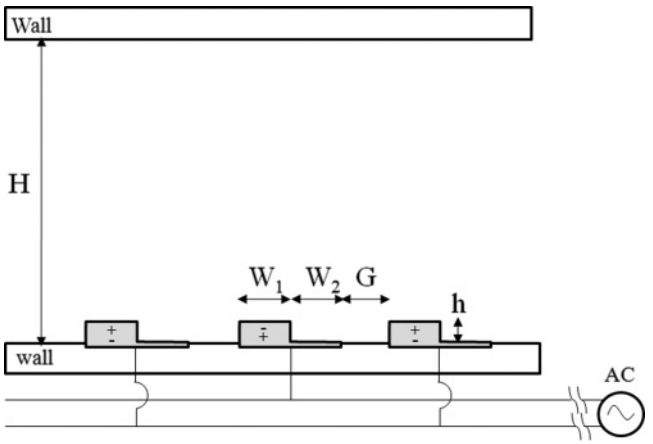

FIG. 1. Schematic of a micropump with step electrodes.

supplied to each pair, a unidirectional flow is formed due to the electro-osmotic force on the fluid. The electrode height and the gap distance between the electrodes are denoted h and G, respectively. The widths of the electrodes are W_1 and W_2. An aqueous 0.001-mol/l KCl solution was used as the working fluid. At room temperature, the electrical conductivity of this solution is $\sigma = 48.9\times^{-3}$ S/m, the electrical permittivity is $\varepsilon = 6.943\times10^{-10}$ F/m, and the viscosity is $\eta = 0.001$ kg^{-1} m^{-2} s^2.

The characteristic parameters for nondimensional analysis are $L_c = G$ (length), $t_c = GC_0\sigma$ (time), $V_c = k_BT/ze$ (potential), $q_c = C_0V_c$ (charge), $u_c = \varepsilon V_c^2/\eta G$ (fluid velocity), and $Q_c = u_cL_c$ (flow rate), respectively. The gap distance is set to the characteristic length. When the gap distance decreases, the electrical field strength increases so that the pumping flow rate increases continuously. The gap distance is $G = 5$ μm, and the dimensionless height is $H^* = H/L_c = H/G = 10$. The asterisk denotes a dimensionless number. The channel height is much greater than the electrode height such that the simulations would not be affected by the channel height. The electrical potential drop and the accumulated charge in the electrical double layer can be described with a capacitor model. $C_0 = \varepsilon/\lambda_D$ is the capacitance of the electrical double layer. Here, λ_D is the Debye length, which is approximately 10 nm for a $c_0 = 0.001$-mol/l solution. The characteristic potential at room temperature (25 °C) is approximately 0.025 V. T, k_B, e, and z are the absolute temperature, the Boltzmann constant, the ion charge, and the ion valence, respectively. The valence of the KCl solution is $z = 1$.

B. Governing equations and numerical methods

Hereafter, unless otherwise stated, the parameters are dimensionless and are based on the characteristic parameters, and the asterisks are omitted. Most of the net charge is present inside the electrical double layer, which is thin compared to the system length. The potential and the charge at the plane where the electrical double layer ends and the bulk region starts are given as boundary conditions to the bulk region simulation. The region inside the electrical double layer is not a matter of concern. Hence, only the bulk region was simulated without any detailed consideration of the region inside the electrical double layer. This requirement means that it is important to use an appropriate model of the thin electrical double layer to ensure as accurate boundary conditions as possible. This approach has been widely used to avoid complicated numerical simulations [2,3,9–11,13,14],

The electrical charge is assumed to be nearly zero in the bulk region,

$$\nabla^2\varphi = 0, \tag{1}$$

where φ is the electrical potential of the electrolyte. Storey *et al.* [9] successfully demonstrated that flow reversal can be predicted in pumps with planar asymmetric microelectrodes, by taking the ion crowding effect due to finite ion sizes into account. In that study, a simple model [15] and a more accurate model [16] were found to give similar results. Therefore, the simple model [15] was used owing to simplicity in the present paper. The original Poisson-Nernst-Planck model was modified to account for the steric effects, leading to the following relation between the potential drop (ψ) and the electrical charge (q),

$$\psi = -2\mathrm{sgn}(q)\sinh^{-1}\left[\sqrt{\left(\frac{1}{2\upsilon^*}\left(e^{[(1/2)\upsilon q^2]}-1\right)\right)}\right], \tag{2}$$

$$\upsilon = 2a^3c_{\mathrm{bulk}} = \left(\frac{a}{l_0}\right)^3, \tag{3}$$

where a, c_{bulk}, and l_0 are the ion size, the solution concentration, and the mean distance between ions, respectively. The dimensionless parameter υ can be determined by fitting numerical simulations to experimental results. In the present paper, $\upsilon = 0.01$ was chosen following the previous result for planar asymmetric electrodes [9]. Note that, in the case of infinitesimally small ions ($\upsilon \to 0$), Eq. (2) becomes the linear model, in which (ψ) is in proportion to q.

As for ψ and q, they are defined only at the electrode surface,

$$\varphi = V_{\mathrm{ext}} - \psi, \tag{4}$$

$$\frac{dq}{dt} = \frac{\partial\varphi}{\partial n}, \tag{5}$$

$$V_{\mathrm{ext}} = V_0\sin(\Omega t), \tag{6}$$

where V_{ext} and n denote the external voltage and the unit vector normal to the electrode surface, respectively. An insulation condition is applied to the channel wall,

$$\frac{\partial\varphi}{\partial n} = 0. \tag{7}$$

Periodic conditions are imposed between the inlet and the outlet.

After solving the electrical equations, Eqs. (1)–(7), the slip velocity of the fluid at the electrode surface is computed as

$$u_{\mathrm{slip}} = \psi\frac{\partial\varphi}{\partial s}, \tag{8}$$

where s is the unit vector tangential to the surface. The fluid flow is then obtained by solving the Stokes equation for low Reynolds numbers,

$$0 = -\nabla p + \frac{1}{\mathrm{Re}}\nabla^2 \mathbf{u}, \tag{9}$$

where p, $\mathbf{u}$, and Re are the pressure, the velocity vector, and the Reynolds number, respectively.

Due to the absence of an inertia term in the Stokes equation, the fluid velocity field changes at once in response to the slip velocity. Moreover, due to the linearity of the Stokes equation, the fluid velocity changes relative to the slip velocity. Consequently, the time-averaged fluid velocity field is equivalent to the fluid velocity field induced by the time-averaged slip velocity. Therefore, the time-averaged fluid velocity field can be obtained without having to solve for the unsteady fluid flow. The time-averaged slip velocity was calculated over two periods after a transient behavior disappears. As for the electrical simulation, periodic conditions were set between the inlet and the outlet. Since a discontinuity problem arose at the electrode edges, a finer mesh was applied to the edges.

III. RESULTS AND DISCUSSION

The present model should be able to predict the experimental behavior of a pump as accurately as possible. Storey *et al.* [9] demonstrated that the results of this model are in good agreement with experimental observations for planar asymmetric electrodes. Thus, a test of the present simulation method was performed for the pump with planar asymmetric electrodes. The time-space-averaged slip velocity over the electrodes is plotted in Fig. 2. The dimensionless parameter for the ion size is $\upsilon = 0.01$, and the voltage amplitude is $V_0 = 100$. Figure 2 shows that there is a maximum at $\Omega = 0.7$ and a minimum at $\Omega = 3.0$. The present data are in fairly good agreement with the reference, which validates the present numerical method.

There are many possible combinations of the geometrical parameters, so we limited our study to cases in which $W = W_1 = W_2$. One of the main goals of the present paper is to determine the geometrically optimized condition for

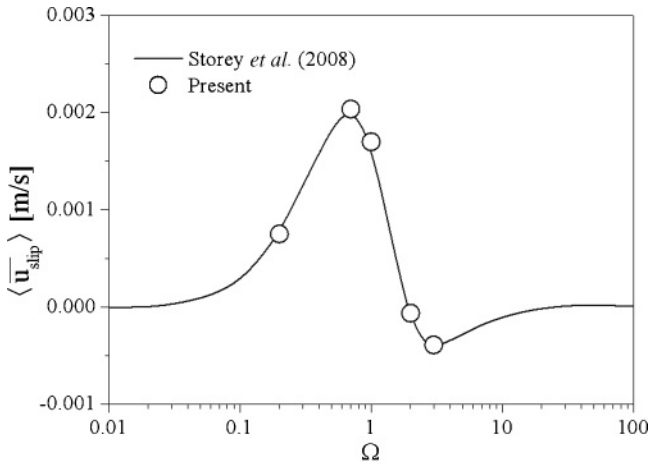

FIG. 2. Validationof the present numerical method.

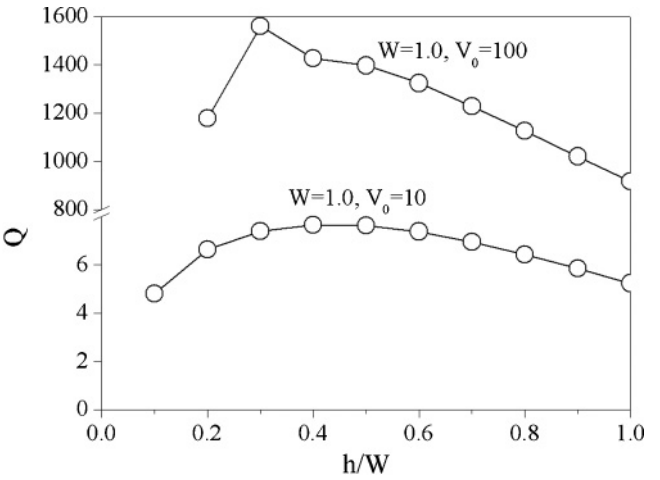

FIG. 3. Variations of the pumping flow rate with the electrode height (h) and the ac amplitude (V_0).

high pumping flow rates. Therefore, simulations started with $\Omega = 1$ since the maximum pumping flow rate is expected to occur near $\Omega = 1$ for ac electrokinetic micropumps [2,3,11]. Figure 3 shows the pumping flow rates for $V_0 = 10$ (0.25 V) and $V_0 = 100$ (2.5 V), while W is fixed at 1. The maximum flow rates occur at $h/W = 0.3$ and $h/W = 0.4$, respectively, in these two cases. Low voltages ($V_0 < 10$) fall into the linear regime. The steric effects on the electrical double layer are present for high voltages. Figure 3 shows that the pumping flow rate is maximized at $h/W = 0.3$–0.4 when the voltage amplitude is higher than moderate values ($V_0 \geqslant 10$). When the electrode height is reduced, the two electrodes become planar and symmetric, leading to symmetric flow. As expected, the pumping flow rate decreases as h/W decreases, as shown in Fig. 3.

Figure 4 shows the variation of the pumping flow rate with the electrode width W. Here, V_0 is fixed at 10. It is evident that, as the electrode width increases, the pumping flow rate decreases; this result is attributed to the increases in the electrical field strength with decreases in the electrode width. In all three cases, the maximum flow rate arises at h/W

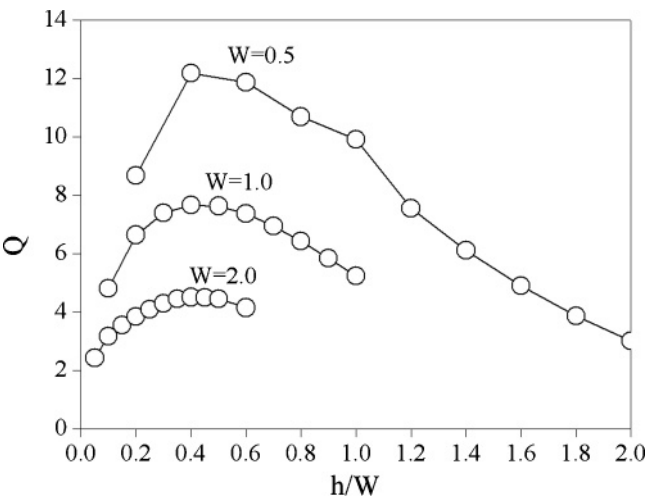

FIG. 4. Variations of the pumping flow rate with the electrode height (h) and the width (W).

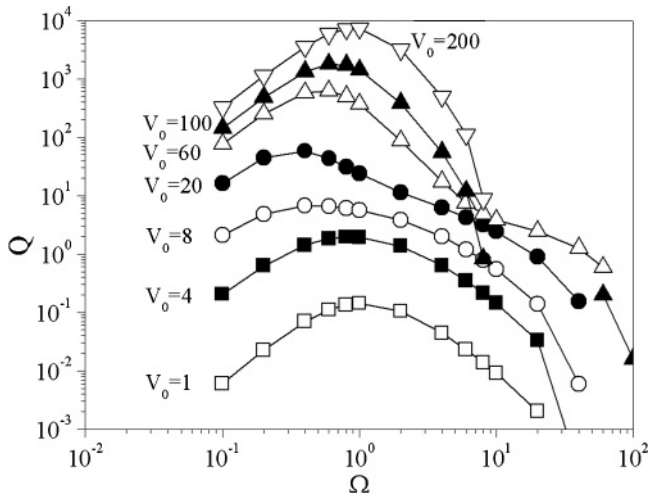

FIG. 5. Variations of the pumping flow rate with the ac amplitude (V_0) and the frequency (Ω).

$= 0.4$, which is consistent with the results in Fig. 3. Thus, the pumping flow rate is maximized at $h/W = 0.3$ or 0.4. This result was also obtained in the previous study with a linear model [11]. The optimal step height is not sensitive to the electrode size or the ac voltage amplitude.

Figure 5 shows the dependences of the amplitude and the frequency on the pumping flow rate. The geometrical dimensions of the electrode are $h/W = 0.4$ and $W = 1$, which were selected because $h/W = 0.4$ yields a nearly maximum flow rate. As shown, the optimal frequency is in the range of $\Omega = 0.7$–1.0, and the maximum pumping flow rate increases with increasing voltage amplitude. Figure 6 enlarges the high frequency region in Fig. 5. In Fig. 6, it is found that the pumping flow rate is considerably low for $\Omega \geqslant 10$ and $V_0 < 100$. For $\Omega \geqslant 10$ and $V_0 \geqslant 100$, flow reversal (backward pumping) is observed on the contrary, but the magnitude is not so high. According to Refs. [11,12], two peak frequencies appear at high voltages. However, such a double-peaked frequency response is not observed throughout simulations. As mentioned in Ref. [6], although the steric effect

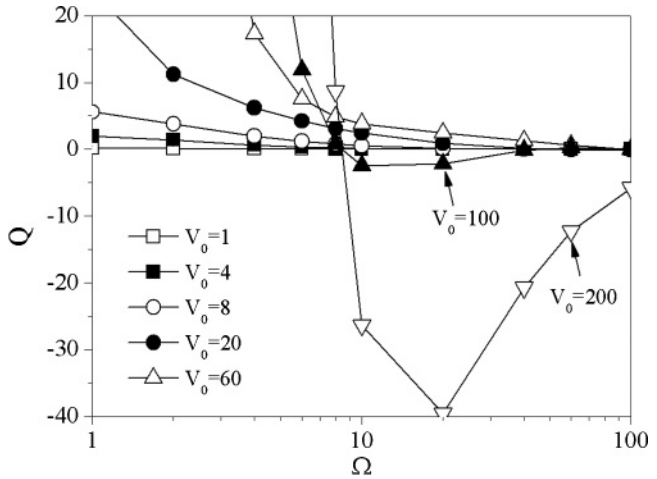

FIG. 6. Variations of the pumping flow rate with the ac amplitude (V_0) and the frequency (Ω).

cannot avoid the salt adsorption at very high voltages, an upper bound on the applied voltage exists such that the circuit model is valid. This will be discussed in the last part of this section.

Figures 5 and 6 can be summed up in the following two points. The first is that the pumping flow rate for $\Omega = 0.7$–1.0 increases with increasing voltage amplitude. For a pump with planar asymmetric electrodes, even when Ω is close to unity, the pumping flow rate decreases with increasing voltage amplitude if the amplitude is higher than a certain value [9]. In order to clarify this behavior of the step electrodes, the slip velocity profile at the electrode surface and the flow structure were examined. Figure 7 shows the fluid velocity fields and the time-averaged slip velocity profiles at $\Omega = 1$ for $V_0 = 10$ and $V_0 = 100$, respectively. The velocity fields are displayed only for $y = 0$–3, and the vectors are scaled. Note that the two velocity fields have a similar pattern, owing to the similar shapes of the two slip velocity profiles. In Fig. 7(a), the positive slip velocities at the higher electrode surface ($x = 0.5$–1.5, $x = 3.5$–4.5) make a significant contribution to positive pumping. On the other hand, the negative slip velocities at the lower electrode surface ($x = 1.5$–2.5, $x = 4.5$–5.5) do not affect negative pumping because of flow blocking by the vertical electrodes. Hence, as the applied voltage increases, the positive slip velocity induces higher forward pumping, but the negative slip velocity does not have a significant effect on backward

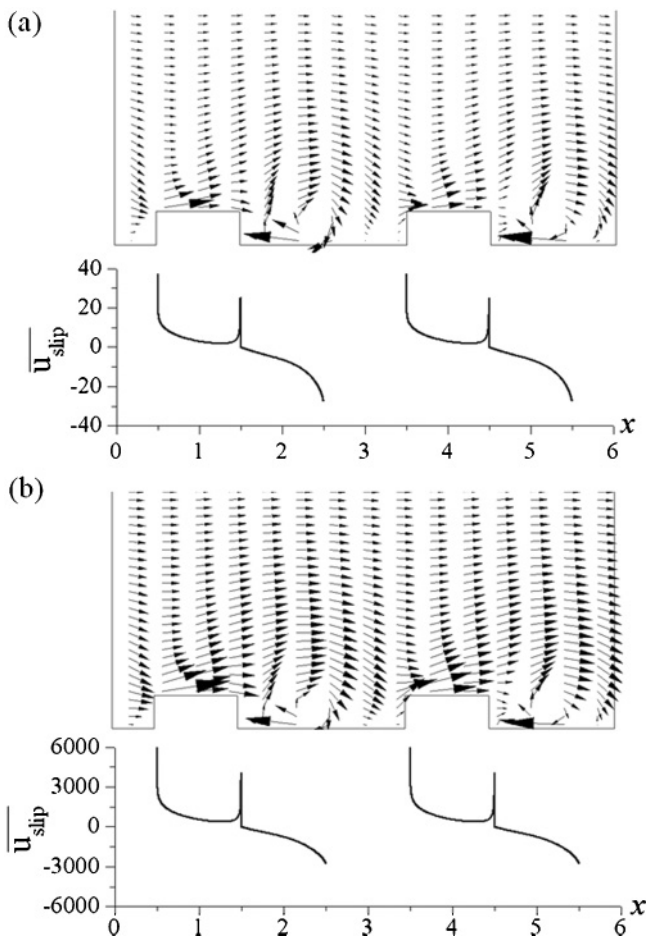

FIG. 7. Time-averaged slip velocity and flow velocity field for forward pumping: (a) $\Omega = 1$ and $V_0 = 10$, (b) $\Omega = 1$ and $V_0 = 100$.

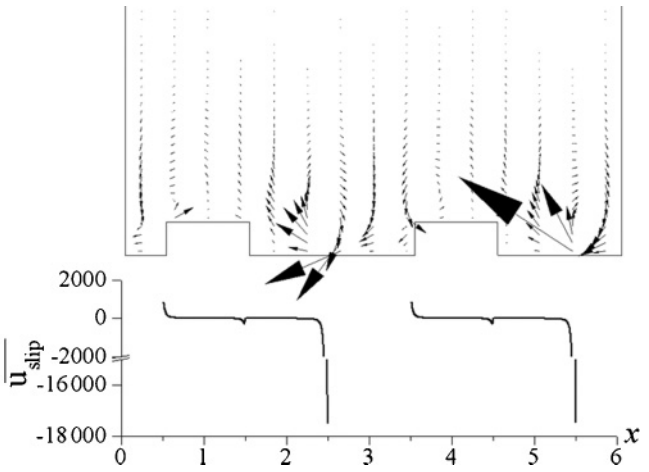

FIG. 8. Time-averaged slip velocity and flow velocity field for backward pumping ($\Omega = 20$ and $V_0 = 200$).

pumping. As a result, the pumping flow rate increases with the amplitude of the applied voltage.

The other point is that backward pumping occurs for high frequencies ($\Omega > 10$) and high amplitudes ($V_0 = 100$,200), although its magnitude is not so high. The fluid velocity field and the slip velocity profile are shown for $\Omega = 20$ and $V_0 = 200$ in Fig. 8. The fluid velocity field is shown only in the range of $y = 0$–3. Note that strong negative slip velocities occur at the edges of the electrodes ($x = 2.5$,5.5) and that the positive slip velocities are relatively small. As a result, the strong negative slip velocities induce backward pumping despite the presence of the vertical surface. The previous study [11] with a linear model showed that flow reversal occurs in the cases of low step electrodes, which is to be expected since the electrode becomes planar as the step height is reduced. As shown in Fig. 6, the flow reversal comes to a standstill as the frequency is increased further, which is physically correct.

Figures 9 and 10 show the variations of the time-averaged slip velocity profiles with the frequency. The voltage amplitude is $V_0 = 200$, and the frequencies are above unity. The arrows

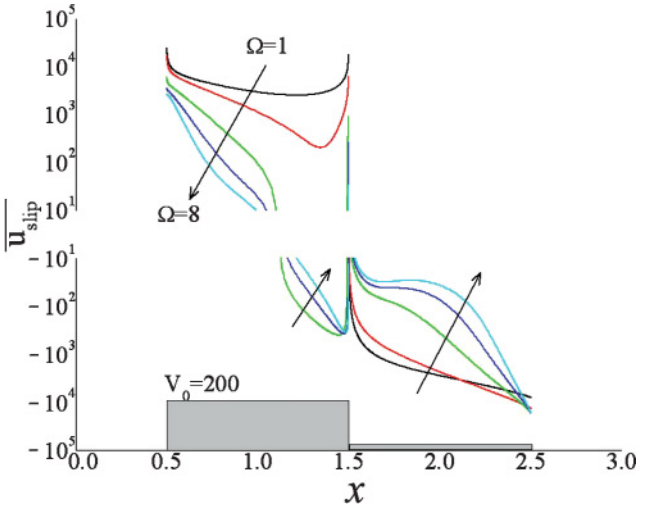

FIG. 9. (Color online) Variation of the time-averaged slip velocity profile with the frequency ($\Omega = 1$,2,4,6,8).

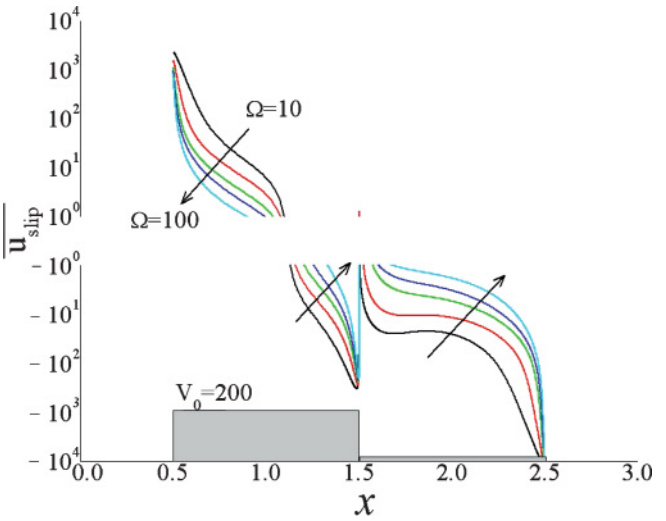

FIG. 10. (Color online) Variation of the time-averaged slip velocity profile with the frequency ($\Omega = 10$,20,40,60,100).

indicate the direction of increasing frequency. As mentioned above, for low frequencies $\Omega \leqslant 1$, the shapes of the slip velocity profiles are similar (see Fig. 7 for an example). However, as can be seen in Figs. 9 and 10, the shapes are no longer similar for high frequencies, and negative slip velocities arise at the upper right surface ($x = 1.0$–1.5) for $\Omega \geqslant 4$. The slip velocity tends to occur mostly at the electrode edges as the frequency increases, which is why the pumping slows when the frequency is very high. This means that negative slip velocities tend to occur mostly at the electrode edges at higher frequencies, causing the pumping to slow at very high frequencies.

Simulations were performed with the linear model for comparison. As mentioned in Sec. II B , unless the steric effect is considered, ψ is proportional to q; Eq. (2) then simplifies to $\psi = -2\mathrm{sgn}(q)\sinh^{-1}(q/2)$ as $\upsilon \to 0$. The governing equations and boundary conditions are the same as those in the nonlinear analysis, except for Eq. (2). Figure 11 shows the pumping flow rate normalized by the square of the ac amplitude. It is evident that the pumping flow rate is exactly proportional to the square of the ac amplitude, and that the optimal frequency is independent of the ac amplitude. These

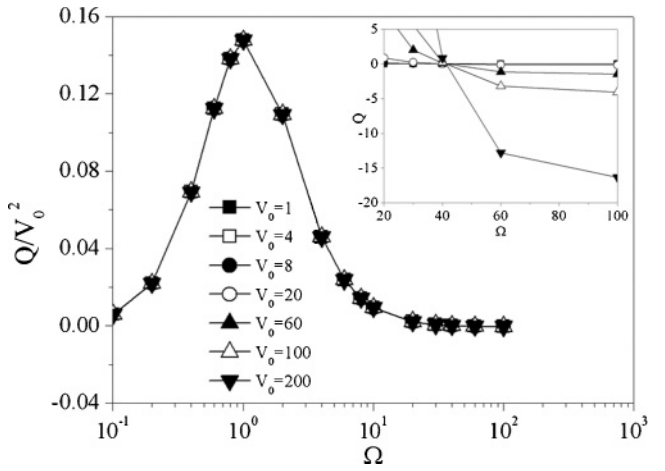

FIG. 11. Results of the linear model for the electrode double layer.

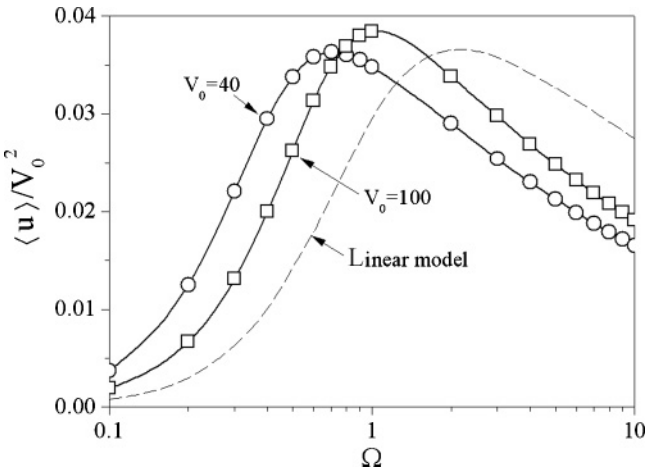

FIG. 12. Simulation results for the step geometry of Burch and Bazant [13].

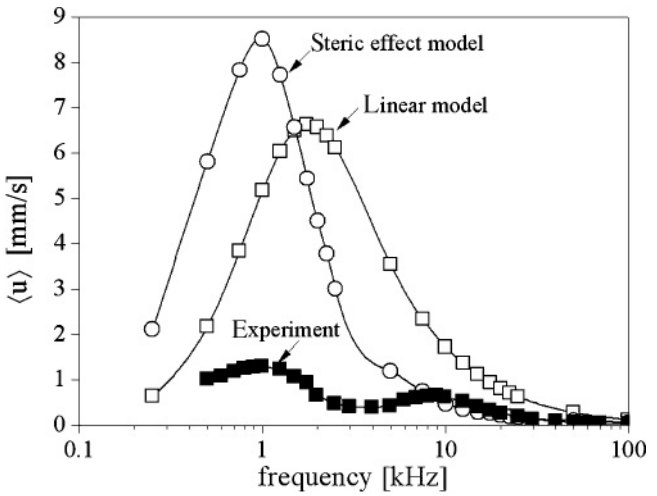

FIG. 13. Comparison of the present simulation with the experiment [12].

behaviors are due to the complete linearity of the system. Different behaviors appear at high frequencies in Figs. 5, 6, and 11: Beyond $\Omega = 1$, the pumping flow rates decrease more rapidly for the nonlinear cases (Fig. 5) than for the linear cases (Fig. 11). For the linear cases, backward pumping occurs whenever the frequency is higher than $\Omega \geqslant 20$, and backward pumping still persists even for a very high frequency, $\Omega = 100$. In a physical sense, fluid cannot respond to such a high frequency, and the electrical double layer does not have enough time to form. Accordingly, the present nonlinear model simulates flow behaviors more realistically.

The steric effect model has been applied to the step electrodes in the present paper. This approach could be applied to a pump with the step geometry whose side vertical wall is not polarized but is an insulating surface. This pump is known to attain the pumping flow rate twice as fast as the pump with entirely polarized step electrodes. The results by the linear and nonlinear models are plotted in Fig. 12. The step geometry is the same as the geometry in Burch and Bazant [13]. The linear model shows high flow rates beyond $\Omega = 1$. The maximum magnitudes for the three cases are similar to one another, however, the optimal frequency shifts to a lower frequency at a moderate voltage $V_0 = 40$. Such behavior can be found in Fig. 5.

Meanwhile, Huang *et al.* [12] realized an ultrafast and high-pressure pump with step electrodes, by placing a large number of electrode pairs on the bottom wall. We compared the experiment with the present simulation. In the experiment [12], the channel width is not much greater than the channel height. In the simulation, however, the effect of the side walls of the channel is neglected. A back pressure exists across the pumping part due to the hydraulic resistance on the nonpumping part. The simulation does not consider the hydraulic resistance on the nonpumping part. Therefore, periodic boundary conditions are imposed between the inlet and the outlet. Figure 13 shows a comparison between the experiment and the simulation. Since the conductivity of de-ionized water in the experiment was not explicitly given in Huang *et al.* [12], the frequency in the simulation is scaled such that the peak frequency for the steric effect model is close to the experimental value. The simulation velocities are the average velocities at the outlet. The applied voltage V_0 is 60 (1.5 V) at which two peak frequencies apparently appear in the experiment. The ion-crowding effect model as well as the linear model overpredict the velocities. The differences between the experiment and the two models are not very large in the magnitude, within 1 order. As mentioned in Ref. [8], the overprediction in velocity may be attributed to the absence of the viscoelectric effect that the liquid viscosity increases with increasing concentration in the double layer. This viscoelectric effect should be modeled in combination with the steric effect. The differences between the experiment and the simulation can be reduced by considering the ratio of the diffuse double layer impedance to the total double layer impedance. The presence of the stern layer reduces the voltage drop across the diffuse layer, accordingly, decreasing the fluid velocity [2,11]. In general, the optimal frequency is overestimated when the linear model is used [2,11]. However, the peak frequency for the ion-crowding effect is about half of the peak frequency for the linear model, as can be seen in Fig. 13. This behavior is also observed at moderate voltages in Figs. 5, 11, and 12. The double-peaked frequency response is not observed in the simulation. The steric effect model does not suffice for a strong nonlinear regime beyond a moderate voltage.

Killic *et al.* [6,7] discussed the condition in which the circuit models break down at large voltages. For the standard Poisson-Boltzmann equations, the salt adsorption increases exponentially with the applied voltage. As a result, the circuit models break down even at low voltages due to a depletion of ions in the bulk. However, as mentioned in Killic *et al.* [6], the steric effect greatly reduces the capacity to pack ions into the double layer due to the finite sizes of ions. This is one of the important advantages of the steric effect model. However, this model still has an upper bound on the applied voltage in which this circuit model is valid. The circuit model is theoretically valid when a crude estimation is satisfied as follows:

$$\frac{w}{c_0}\sqrt{\frac{2\omega}{D}} = \frac{w}{2c_0\lambda_D}\sqrt{\frac{8\omega\lambda_D^2}{D}} = \frac{w}{2c_0\lambda_D}\sqrt{\frac{8\omega t_c \lambda_D}{G}} \ll 1. \tag{10}$$

Here, the parameters in Eq. (10) have dimensions. The salt adsorption w is calculated using Eq. (36) in Killic *et al*. [6], and D is the ion diffusivity. The dimensionless salt adsorption $w/(2c_0\lambda_D)$ must be less than 7.9, for example, for $\Omega = \omega t_c = 1$, $G = 5$ μm and $\lambda_D = 10$ nm, $\upsilon = 0.01$. This value corresponds to the upper voltage $V_0 \approx 8$ (0.2 V). However, when the stern layer is considered, the upper bound on the applied voltage becomes larger than 0.2 V. Although the steric effect model is more realistic than the linear model, a more accurate understanding is needed, which is related to full modified Poisson-Nernst-Planck equation rather than the circuit model and the thin Debye layer approximation [6].

IV. CONCLUSIONS

Numerical simulations of a pump with step electrodes have been performed, with the aim of investigating the effects on the pumping flow rate of varying the geometrical parameters and the ac voltage. To this end, a more realistic model that accounts for the finite sizes of ions (the steric effect) was used. The pumping flow rate is maximized at $h/W = 0.3$ or 0.4, and this maximum is not sensitive to the electrode size or the ac voltage amplitude. The pumping flow rate increases with voltage amplitude when $\Omega = 0.7$–1.0 since the shape of the slip velocity profile then remains largely independent of the voltage amplitude. However, the optimal frequency varies between $\Omega = 0.7$–1.0 depending on the voltage amplitude. For high frequencies ($\Omega > 10$) and high amplitudes ($V_0 = 100$,200), backward pumping is observed due to strong negative slip velocities at the electrode edges. As Ω is increased further, however, backward pumping comes to a standstill. These results were achieved by using a nonlinear model for the electrical double layer. The linear model predicts that the optimal frequency will be independent of the ac voltage amplitude and that backward pumping will persist even at very high frequencies. Although this model is more realistic than the linear model, it was not able to predict two peak frequencies that appear at large voltages. This might be attributed to a strong nonlinear regime at high voltages where the circuit model is not valid.

ACKNOWLEDGMENTS

This study was supported by the Creative Research Initiatives (Grant No. 2011-0000433) of the National Research Foundation of Korea.

[1] B. Iverson and S. Garimella, Microfluid. Nanofluid. **5**, 145 (2008).
[2] A. Ramos, A. González, A. Castellanos, N. G. Green, and H. Morgan, Phys. Rev. E **67**, 056302 (2003).
[3] L. H. Olesen, H. Bruus, and A. Ajdari, Phys. Rev. E **73**, 056313 (2006).
[4] V. Studer, A. Pepin, Y. Chen, and A. Ajdari, Analyst (Cambridge, UK) **129**, 944 (2004).
[5] M. M. Gregersen, L. H. Olesen, A. Brask, M. F. Hansen, and H. Bruus, Phys. Rev. E **76**, 056305 (2007).
[6] M. S. Kilic, M. Z. Bazant, and A. Ajdari, Phys. Rev. E **75**, 021502 (2007).
[7] M. S. Kilic, M. Z. Bazant, and A. Ajdari, Phys. Rev. E **75**, 021503 (2007).
[8] M. Z. Bazant, M. S. Kilic, B. D. Storey, and A. Ajdari, New J. Phys. **11**, 075016 (2009).
[9] B. D. Storey, L. R. Edwards, M. S. Kilic, and M. Z. Bazant, Phys. Rev. E **77**, 036317 (2008).
[10] M. Z. Bazant and Y. Ben, Lab Chip **6**, 1455 (2006).
[11] J. P. Urbanski, J. A. Levitan, D. N. Burch, T. Thorsen, and M. Z. Bazant, J. Colloid Interface Sci. **309**, 332 (2007).
[12] C.-C. Huang, M. Z. Bazant, and T. Thorsen, Lab Chip **10**, 80 (2010).
[13] D. Burch and M. Z. Bazant, Phys. Rev. E **77**, 055303 (2008).
[14] B. J. Kim, S. Y. Yoon, H. J. Sung, and C. G. Smith, J. Appl. Phys. **102**, 074513 (2007).
[15] J. J. Bikerman, Philos. Mag. **33**, 384 (1942).
[16] N. F. Carnahan and K. E. Starling, J. Chem. Phys. **51**, 635 (1969).